From Ultrananocrystalline Diamond to Single Crystal Diamond Growth in Hot Filament and Microwave Plasma-Enhanced CVD Reactors: a Unified Model for Growth Rates and Grain Sizes

Paul W. May*,† and Yuri A. Mankelevich‡

School of Chemistry, University of Bristol, Bristol, BS8 1TS, U.K., and Nuclear Physics Institute, Moscow State University, 119991 Moscow, Russia

Received: April 29, 2008

CVD Diamond can now be deposited either in the form of single crystal homoepitaxial layers, or as polycrystalline films with crystal sizes ranging from mm, μm or nm, and with a variety of growth rates up to 100s of μm h^{-1} depending upon deposition conditions. We previously developed a model which provides a coherent and unified picture that accounts for the observed growth rate, morphology, and crystal sizes, of *all* of these types of diamond. The model is based on competition between H atoms, CH_3 radicals and other C_1 radical species reacting with dangling bonds on the diamond surface. The approach leads to formulas for the diamond growth rate G via mono and biradical dimer sites and for the average crystallite size $<d>$, that use as parameters, the substrate temperature and the concentrations of H and CH_x ($0 \le x \le 3$) near the growing diamond surface. We recently added a correction factor to the equation for $<d>$ and we now test the predictions of this new equation for diamond crystallite sizes ranging from 10 nm (ultrananocrystalline diamond) to several mm (for single crystal diamond). We find that our model predicts the growth rates of all the forms of diamond to within a factor of 2, and predicts crystal sizes for the growth from CH_3 that are consistent with those seen experimentally. We deduce that growth of diamond is a sliding scale, with different types of diamond arising from a smoothly changing ratio of atomic H to hydrocarbon radical concentrations $[H]:\Sigma CH_x]$ at the growing surface. The different growth conditions, gas mixtures, temperatures and pressures reported in the literature for diamond growth, simply serve to fix the value of this ratio, and with it, the resulting film morphology and growth rate. In general, for conditions of high [H] at the surface, diamond growth is predominantly from CH_3 addition to monoradical sites, leading to large crystals (or even single crystal growth). With decreasing $[H]/[CH_3]$, a competing growth channel emerges whereby CH_3 adds to biradical sites and the average crystallite size is reduced simultaneously to μm or even nm for very low $[H]/[CH_3]$ ratio. In a third growth channel involving atomic C adding to either mono or biradical sites, the spare 'dangling bond' can promote renucleation events and increase possibilities for cross-linking, leading to even smaller nm-sized crystallites. This channel can be dominant in high temperature reactors (e.g., MW plasma-enhanced CVD in $1\%CH_4/(0-2\%)H_2/Ar$ mixtures) where high hydrogen dissociation degree shifts the population distribution in CH_x group in favor of C atoms.

1. Introduction

Diamond films can be deposited using a chemical vapor deposition (CVD) process involving the gas phase decomposition of a gas mixture containing a small quantity of a hydrocarbon in excess hydrogen.[1] A typical gas mixture uses $1\%CH_4$ in H_2, and this produces polycrystalline films with grain sizes in the micron or tens of micron range, depending upon growth conditions, substrate properties and growth time. It is generally believed [2,3] that the main growth species in standard diamond CVD is the CH_3 radical, which adds to the diamond surface following hydrogen abstraction by H atoms. Thus, a high concentration of atomic H at the surface in addition to CH_3 radicals is a prerequisite for successful microcrystalline diamond (MCD) deposition. By increasing the ratio of methane in the standard CH_4/H_2 gas mixture from 1% to ~5%, the grain size of the films decreases, and eventually becomes of the order of hundreds down to tens of nm. Such nanocrystalline diamond (NCD) films (often termed 'cauliflower' or 'ballas' diamond) are smoother than the microcrystalline ones, but have larger numbers of grain boundaries that contain substantial graphitic impurities. With further addition of CH_4 the films become graphitic.

Ultrananocrystalline diamond (UNCD) films offer the possibility of making smooth, hard coatings at relatively low deposition temperatures, which can be patterned to nm resolution.[4,5] These differ from NCD films[6] since they have much smaller grain sizes (~2−5 nm). Most reports of the deposition of these films describe using a microwave (MW) plasma-enhanced (PE) CVD reactor and gas mixture of $1\%CH_4$ in Ar, usually with addition of 1−5% H_2.[4] We have previously reported the use of similar $Ar/CH_4/H_2$ gas mixtures to deposit NCD (or UNCD) in a hot filament (HF) reactor,[7] with the compositional diagram for mixtures of Ar, CH_4 and H_2 being mapped out corresponding to the type of film grown. Originally, it was suggested[8] that the C_2 radical played an important role in the growth mechanism for UNCD. However, recent work

* To whom correspondence should be addressed. E-mail: paul.may@bris.ac.uk.
† University of Bristol.
‡ Moscow State University.

10.1021/jp803735a CCC: $40.75 © 2008 American Chemical Society
Published on Web 07/23/2008

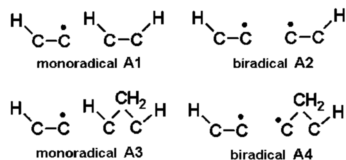

Figure 1. Main types of radical site important for growth on a (100) diamond surface during CVD. The sites are labeled A1, A2, A3, and A4 following the scheme of Skokov et al.[20]

by ourselves [9,10] and others[11] has shown that C_2 is not a dominant species close to the substrate surface.

At the other end of the scale, single crystal diamonds (SCD) up to several carats (1 carat = 0.2 g) in weight have recently been successfully grown in high power MW PECVD reactors using 1%−12%CH_4/H_2 mixtures, sometimes with small additions of N_2 or O_2. For example, 270 μm-thick single crystal diamond films of area of 2.5 × 2.5 mm have been grown by the group at Hasselt University at 700 °C using 10%CH_4 in H_2.[12] The same group reported epitaxial diamond growth yielding sub-nm smooth surfaces for films with thicknesses up to 730 μm at growth rates of $G \approx 3-4$ μm h^{-1}.[13] Using similar conditions, freestanding diamond films of area 4 × 4 mm^2 and thickness between 390−690 μm were reported by workers from Element Six.[14] Recently, a group based at the Carnegie Institute in Washington have grown single crystal diamond up to 4.5 mm in thickness at growth rates ($G \approx 50-150$ μm h^{-1}) as much as 2 orders of magnitude higher than conventional polycrystalline CVD methods.[15,16] These single crystals can be fashioned into brilliant cut 'gemstones' using standard techniques.

In our previous papers,[10,17,18] we used 2- and 3-dimensional models for simulation of UNCD, NCD and MCD deposition processes in HF reactors and a 2D(r,z) model for SCD growth in high power MW PECVD reactors to understand these experimental observations. Here, we add the calculated and experimental results for UNCD deposition in our MW PECVD reactor and describe in detail a generalized mechanism for UNCD, NCD, MCD and SCD growth that is consistent with many experimental observations, both from our group and from others in the literature.[18]

2. Models for the Growth Mechanisms and Average Crystal Sizes

2.1. Growth from CH_3. The proposed mechanism involves competitive growth by all the C_1 radical species that are present in the gas mixture close to the growing diamond surface. We shall consider the reconstructed (100)-(2 × 1) diamond surface for the basis of all the growth models because growth on this surface is the most commonly studied. Experimentally, it has been found[19] that under the same conditions the growth rates on many diamond surfaces, e.g., (100), (111) (110), (113) are very similar to each other (often less than a factor of ∼2 difference), which suggests that our derived growth rate formulas for the (100)-(2 × 1) surface are valid for other diamond surfaces, including randomly oriented polycrystalline diamond, within a factor ∼2. In most growth models, abstraction of surface H atoms by gas phase atomic H are the reactions which drive the chemistry of growth. These reactions create two main types of surface radical sites on the reconstructed (100)-(2 × 1) diamond surface[20] (see Figure 1), monoradical sites (a single dangling bond on a surface carbon) and biradical sites (defined as two surface radical sites on adjacent carbons). There are different variants of these bi- and monoradical sites, depending upon the local surface geometry, and the most important for growth have

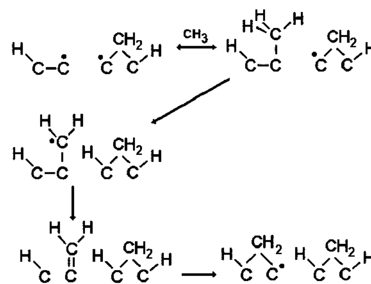

Figure 2. Example of a possible reaction following CH_3 addition to a biradical A4 site. The adjacent dangling bond is already present, so linking of the CH_3 group into the lattice occurs rapidly.

been labeled as A1, A2, etc., in Figure 1. For typical diamond CVD conditions, the fraction of available biradical sites (of all types) is ∼10 times lower than that of the monoradical sites (see below).

According to quantum-mechanical calculations[20] for a diamond (100) surface, CH_3 can add to dimer sites (both mono and biradical) but CH_3 cannot add to bridge and dihydride surface sites because of the strong steric repulsion among H atoms of the CH_3 group and the surrounding surface H atoms. In our model we consider the addition of CH_3 to both biradical dimer sites [9,10,18] and to monoradical dimer sites[17] as the primary processes by which carbon is added to the diamond lattice. The total growth rate results from the combination of these two processes, while the overall film morphology could be dependent upon the branching ratio between these two channels.

a. CH_3 Addition to Biradical Sites. Since the biradical sites have an adjacent dangling bond already present, the CH_3 adduct does not have to wait for a suitable abstraction reaction to occur before it can link into the lattice (see Figure 2). Thus, the reaction that forms a bridging CH_2 group readily occurs before the CH_3 can desorb. In refs [18,21,22] we derived an equation for the growth rate contribution, G (in μm h^{-1}) from CH_3 via this biradical channel as

$$G_{bi} = 3.8 \times 10^{-14} T_s^{0.5} [CH_3] R^2 \quad (1)$$

where T_s is the substrate temperature in K and R is the fraction of surface monoradical sites (see below). The growth rate is proportional to the flux of the gas-phase diamond precursor (e.g., CH_3) at the substrate, which we assume can be expressed as $[CH_3]\upsilon_T/4$, where υ_T is the average thermal velocity of methyl and $[CH_3]$ is the concentration of CH_3 *at* the surface, which is calculated using the procedure outlined in Sections 3 and 3.1.b.

b. CH_3 Addition to Monoradical Sites. CH_3 can also attach to monoradical dimer sites,[20,23] thereby terminating the single 'dangling bond' and forming a pendant CH_3 adduct (see Figures 3 and 4). There are then two competing processes which determine the fate of this adduct. One is that the adduct can simply desorb back into the gas phase (which is likely to be quite a facile process) and reform the monoradical site, and this can be quantified by a desorption rate, k_d. Alternatively, a suitable H abstraction reaction might occur on a neighboring lattice position (or on an H atom from the CH_3 adduct) during the time the CH_3 remains attached to the surface, followed by fast H atom transfer from the pendant CH_3 to this vacant site.[20] This H abstraction reaction would depend upon the gas-phase atomic hydrogen concentration above the surface, [H], and the rate would be given by k_a[H], where k_a is the rate constant for abstraction. Then, the pendant CH_2 will create a dangling bond on the adjacent carbon of the same dimer via a β-scission reaction (last two stages in Figures 2–4) and thus, the pendant

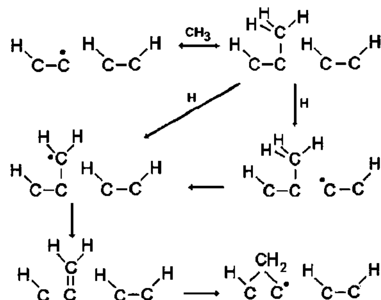

Figure 3. Possible reactions following CH_3 addition to a monoradical A1 site. The CH_3 can desorb, or a subsequent H abstraction reaction can create a dangling bond (either on an adjacent C or on the CH_2 group itself), allowing the carbon to link, adding to the lattice as a bridging CH_2 group.

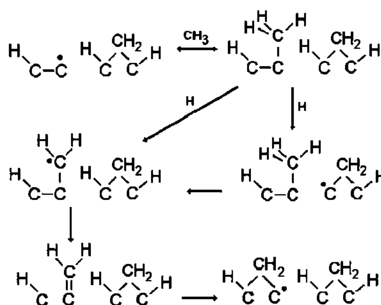

Figure 4. Possible reactions following CH_3 addition to a monoradical A3 site. The CH_3 can desorb, or a subsequent H abstraction reaction can create a dangling bond (either on an adjacent C or on the CH_2 group itself), allowing the carbon to link, adding to the lattice as a bridging CH_2 group.

CH_2 will be incorporated into the lattice as a bridging CH_2 group. Therefore, for successful incorporation of CH_3 into the diamond lattice via monoradical sites, the rate of H abstraction must be comparable with or higher than the CH_3 desorption rate, i.e., $k_a[H] \geq k_d$. We have included this mechanism[17] into our model by adding two monoradical channels to compete with the biradical growth rate given by eq 1. These channels involve two main monoradical sites during regular growth, a dimer−dimer pair (A1 in Figure 1) and a dimer-bridge pair (A3 in Figure 1) (as mentioned above CH_3 cannot add to bridge and dihydride sites[20]). We also assume that the time-averaged fraction of these sites are 50%, and that the rate of the CH_3 absorption on these monoradical dimer sites is the same as for biradical sites[18] (8.3×10^{-12} cm^{-3} s^{-1} for T_s = 1200 K). To derive an expression for the growth rate, G_{mono}, via monoradical dimer channels similar to that in eq 1, we should change R^2 (the probability of the surface site becoming a *bi*radical site) in eq 1 to R (the probability of the *mono*radical surface site), and multiply by the probability of CH_3 incorporation via monoradical channels, given by $k_a[H]/(k_a[H] + k_d)$. Thus, we will have

$$G_{mono} = 3.8 \times 10^{-14} T_s^{0.5}[CH_3] \times R \times 0.5 \times k_a[H]\{1/(k_a[H] + k_d(A1)) + 1/(k_a[H] + k_d(A3))\} \quad (2)$$

and the total growth rate due to CH_3 can now be expressed as

$$G_{CH3} = 3.8 \times 10^{-14} T_s^{0.5}[CH_3] \times R \times \{0.5 \times k_a[H] \times (1/(k_a[H] + k_d(A1)) + 1/(k_a[H] + k_d(A3))) + R\} \quad (3)$$

where $k_d(A1)$ and $k_d(A3)$ refer to the rates of desorption of CH_3 from A1 and A3 sites, respectively.

c. Estimation of the Fraction of Surface Radical Sites, R. The fraction of surface monoradical sites is given by $R = C_d^*/(C_d^* + C_dH)$, where C_d^* and C_dH are the respective densities of open and hydrogen-terminated surface sites. This fraction, R, mainly depends on the rate constants for the surface H abstraction and addition reactions. Neglecting the effects of CH_x upon radical site density R, we obtain[9]

$$R = 1/\{1 + 0.3 \exp(3430/T_s) + 0.1 \exp(-4420/T_s)[H_2]/[H]\} \quad (4)$$

where [H] and [H_2] are the atomic and molecular hydrogen gas-phase concentrations at the substrate surface, respectively. The percentage of both types of open sites plotted for different substrate temperatures and [H_2]/[H] ratios is presented in ref.[17] These values help to explain the diamond growth behavior observed at different temperatures. At standard CVD growth temperatures of ~1200 K, and values of [H_2]/[H] = 1000 (typical of CVD diamond growth[9]), the fractions of monoradical and biradical sites are about $R \approx 12\%$ and $R^2 \approx 1.4\%$, respectively. The relative contributions for incorporation of CH_3 via monoradical and biradical channels depend mainly on the substrate temperature and on [H]. As can be seen from eqs 1 and 2, the following trends should be observed: high [H] will promote the monoradical channel, whereas higher desorption rates k_d will reduce the monoradical channel contribution.

d. Relative Importance of the Reaction Pathways. The importance of the reaction channel (monoradical or biradical pathway) arises from the following observation drawn from comparison of experimental and calculated results (Section 4): the deposition conditions for which growth is dominated by the monoradical pathway promote growth of large crystals, whereas the conditions for which the biradical pathway is important provide the opportunity for renucleation, leading to a decrease in crystal size. Thus, knowledge of the predominant growth pathway occurring for a given set of deposition conditions should make it possible to estimate the size of the crystallites (see Section 2.3).

We can estimate the relative importance of the monoradical and biradical growth processes for CH_3 for different diamond CVD conditions. Using the values of k_a from ref 18, and $k_d(A1)$ and $k_d(A3)$ from ref 20 for a typical substrate temperature of T_s = 1200 K, we see that CH_3 incorporation rate via the monoradical dimer sites A1 and A3 will be equal to the biradical incorporation rate when $[H] = 2Rk_d(A1)/((1 - R)k_a)$ and $[H] = 2Rk_d(A3)/((1 - R) \cdot k_a)$, respectively. For $R \sim 0.1$ this condition will occur when $[H] = 1.8 \times 10^{14}$ cm^{-3} for the A1 site ($k_d = 5300$ s^{-1} [20]) and when $[H] = 5.2 \times 10^{15}$ cm^{-3} for the A3 site ($k_d = 1.5 \times 10^5$ s^{-1} [20]). It should be noted that the A1 channel (Figure 3) will be the main monoradical pathway of CH_3 incorporation with the assumptions and the values of k_d mentioned above.

Our simulations show that near to the growth surface, $[H] \approx 10^{14}-10^{15}$ cm^{-3} for typical MCD growth conditions in HFCVD and MW PECVD reactors, therefore CH_3 incorporation via biradical and monoradical sites could be comparable for these cases. In contrast, for SCD growth in high power MWCVD reactors $[H] \approx 10^{16}$ cm^{-3}, and thus, CH_3 incorporation via monoradical sites will be the dominant mechanism. However, we note that accurate estimation of the contributions from both channels (mono and biradical) requires reliable values of [H] (and k_d for the monoradical channel) and its substrate temperature dependences.

2.2. Growth from CH_x, x = 0, 1, 2. Previous diamond growth models mainly considered CH_3 since this is the dominant reactive

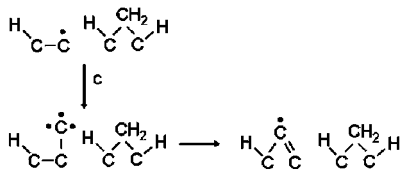

Figure 5. Addition of atomic C to a monoradical A1 site. Once attached, the adduct remains reactive and can react with the surface, linking the carbon into the lattice. However, this linked adduct remains reactive due to its dangling bonds. Unless these dangling bonds are terminated sufficiently rapidly by gas phase H atoms, the adduct may undergo further reactions with the surface, cross-linking to form a surface defect, which may then act as the nucleation point for a new, misoriented crystallite.

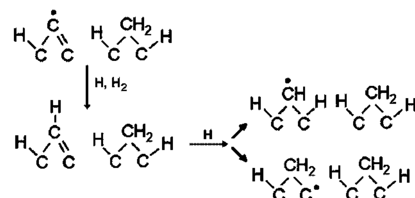

Figure 6. One example of a hydrogenation reaction acting upon the reactive linked adduct from Figure 5, which leads to a CH_2 bridge and subsequent 'normal' diamond growth.

hydrocarbon radical in standard H_2-rich CVD gas mixtures. However, other species may also contribute to diamond growth under certain conditions. C atoms as a gas-phase precursor of diamond films have been considered before for HFCVD,[24] microwave CVD[25] and plasma arc jet reactors.[21,26–28] We found that in multifilament CVD reactors at high filament temperatures (e.g., $T_{fil} \approx 2700$ K)[18] and in MW PECVD reactors for UNCD deposition,[17] the concentration of C atoms near to the growing diamond surface can become comparable to or higher than that of CH_3, and so may contribute to the growth process. Experimental evidence that high C concentrations can occur at the substrate surface comes from mass spectrometric sampling from a flowing MW discharge plasma under low power (30 W) and low pressure (2.2 Torr) nanodiamond deposition conditions, which found that atomic C was the most abundant species, along with C_2H_z ($z = 0-5$).[29] Thus, these species must not be neglected when modeling growth. The sticking coefficients β of various hydrocarbon species C_yH_z ($y = 1-4$) species on diamond (100) 2 × 1 and (111) 1 × 1 surfaces were calculated[30] for (U)NCD conditions by a molecular dynamics method. The highest $\beta \approx 0.8-1$ were observed for C_yH_z with $z = 0$ and 1.

In light of these findings, along with CH_3 addition our growth model assumes that CH_x ($x < 3$) species (C atoms, CH and CH_2 radicals) can also adsorb onto the surface. CH_x species, being more reactive than CH_3, can readily attach to *both* surface monoradical sites and biradical sites. The C and CH radicals also differ from CH_3 in that after bonding to the surface they still have at least one 'spare' dangling bond and thus remain highly reactive. In the case of monoradical sites, once attached, the reactive adduct does not have to wait for a subsequent H abstraction reaction - it simply utilizes its spare dangling bond to react with an adjacent carbon and link into the lattice (see Figure 5). This will also occur on biradical sites in much the same way. Therefore, CH_x species can be readily incorporated into the diamond lattice via both monoradical and biradical sites. The result of this is that even for low CH_x concentrations $[CH_x]/[CH_3] \approx R + k_a[H]/(k_a[H] + k_d)$, their contribution to the growth rate can become important since they can readily add to the more abundant radical sites.

In a similar to manner to eq 2, it is possible to estimate the contribution to the growth rate, G (in μm h^{-1}), of these CH_x species, using formulas stated in refs 18, 21

$$G_{CHx} = 3.9\times10^{-14}T_s^{0.5}[CH_x]R \qquad (5)$$

where CH_x is for $x = 0$, 1, 2.

When does the growth due to C and CH become significant, even in conditions $[C]<[CH_3]$, compared to the usually dominant CH_3 channels? We can answer this question by recalling that the percentage values for R and R^2 are a sensitive function of temperature. For lower temperatures, the number of radical sites (of both types) falls rapidly, and this highlight why diamond CVD is often a slow process under conditions where CH_3 is the only possible growth species. The MCD growth rate, G, has an activation energy $E \approx 20-30$ kcal mol^{-1} ($G \approx \exp(-E/(0.001987T_s))$) at $T_s < 1200$ K,[31] and drops an order of magnitude for each ~200 K decrease in T_s (e.g., for $T_s \approx 1000$, 800 K). The percentage of biradical sites drops accordingly with decreasing T_s and, in addition, CH_3 concentrations are reduced at low temperatures because of three-body recombination of CH_3 with H atoms. Note, however, that UNCD and NCD can be deposited (slowly) in MW PECVD reactors in 1%CH_4/Ar mixtures at temperatures down to ~700 K.[5] Here, C atoms could be the main contributors to growth,[10] because these only require monoradical sites with corresponding activation energy $E \approx 6.9$ kcal mol^{-1} ($G \sim R \sim \exp(-E/(0.001987T_s))$), eqs 4 and 5. R has a small but nonzero value ($R \sim 3\%$), even at these low temperatures: for higher $[H_2]/[H]$ ratios, the value of R^2 at all temperatures is too low for growth by CH_3 alone, but R is sufficient that growth from the other C_1 species is still possible, even down to temperatures as low as $T_s \approx 700$ K. This is consistent with the fact that literature reports of low temperature growth often describe that the films consist of low quality, defective, small grains, with high sp^2 carbon content, and/or NCD-type material.[32,33] It should be noted that experimentally observed values of E are in the range $E \approx 2-8$ kcal mol^{-1}.[5]

2.3. Fate of CH_2 Bridging Groups, and Crystal Size Estimation. We now consider the fate of the bridging CH_2 groups. From the stable bridging structure shown in Figure 3, further hydrogen abstraction reactions allow the CH_2 groups to migrate across the dimer chains[20] until they meet another CH_2 bridge group or a step-edge, at which point they will lock into place, extending the diamond lattice, leading to large regular crystals. In contrast, many of the bridging structures created following addition of C and CH species (as shown in Figure 5) would remain reactive since they still contain at least one dangling bond. The most likely fate for such reactive surface sites, considering that they are surrounded by a gas mixture containing a high concentration of H atoms, is that they are rapidly hydrogenated to CH_2 (Figure 6). If so, the subsequent reactions will be indistinguishable from attachment and growth by methyl, as described above. The rate of these hydrogenation reactions can be estimated by reference to an analogous gas phase reaction, such as: $C_2H_4 + H + M \rightarrow C_2H_5 + M$. The high-pressure limit of this reaction rate is $k[M] \approx 5 \times 10^{-12}$ cm^3 s^{-1} at $T \approx 1000$ K.[34] The characteristic time of this reaction (given by $\tau \approx (k[M][H])^{-1}$) for typical MCD growth conditions ($[H] \approx 2 \times 10^{14}$ cm^{-3}, $[CH_3] \approx 10^{13}$ cm^{-3}, $T_s = 1200$ K and $R \approx 0.1$) is $\tau \approx 1$ ms, which is comparable with the characteristic time for H abstraction $\tau \approx (k_a[H])^{-1} \approx 0.8$ ms and much lower than that for CH_3 adsorption $\tau \approx (k_{ad}[CH_3]R)^{-1} \approx 120$ ms.

When the atomic H concentration is low, other fates for the reactive surface adducts become possible, such as reaction with other gas-phase hydrocarbon radicals (such as CH_x and more

complex species C_yH_z, $y > 1$), further bridging, or cross-linking, which may lead to restructuring of the surface, or even renucleation of a new, misoriented crystallite. These processes are proposed to be one route by which the size of crystallites is prevented from becoming larger. In any case, these processes as well as the probability and feasibility of reactions pathways shown in Figures 5 and 6 require additional study and special quantum-mechanical calculations.

For the typical conditions used to deposit MCD/NCD and UNCD in a variety of different diamond CVD reactors (including MW and HF CVD reactors), the reactions of the surface adducts with atomic hydrogen which lead to continuous normal diamond growth are much more frequent events than the surface reactions which might ultimately lead to renucleation. So long as the surface migration of CH_2 (induced by H abstractions) is much faster than adsorption of CH_3, the aggregation of CH_2 bridge sites into continuous chains (void filling) will provide normal layer-by-layer {100} diamond growth.[20] But as the ratio of gaseous CH_x/H increases, the initiation of next layer growth could proceed before all the voids in the current layer are filled. Thus, the average equilibrium crystal sizes, $<d>$, and hence the morphology of the subsequent film, will depend upon the relative concentrations of various species (H, H_2, CH_x, C_yH_z) close to the growing diamond surface, the probability of the renucleation events, and the deposition and predeposition conditions (e.g., nucleation density).

Comparing the frequency of CH_2 surface migration processes with those for CH_x addition we previously derived[18] quantitative estimates from the equation $<d> \sim [H]/\Sigma[CH_x]$, where $x = 0-3$. A closer approximation of the average migration length from random walk theory results in a square-root ($<d> \sim ([H]/\Sigma[CH_x])^{0.5}$) dependence.[35] However, both these predictions provide a much less variable and narrower range of $<d>$ than is observed experimentally.[17] It may be that there is no universal expression for $<d>$ that works well over such a wide range from nm (UNCD) to mm (SCD). Nevertheless, we proposed[17] a semiempirical extension of the formula for $<d>$ which could at least provide a first approximation to crystal size. Taking into account renucleation due to CH_x and C_yH_z, an equation for the average crystal size $<d>$ in nm can be given in the following general form:

$$<d> = \{2 + 0.6\exp(3430/T_s)\} \times \{[H]/\Sigma[CH_x]\}/\{\Sigma f_{1x}([CH_x]) + \Sigma f_{2yz}([C_yH_z])\} \quad (6)$$

Here, f_1 and f_2 are 'efficiency functions' which determine how efficient these defect creation processes are, and the subscripts x,y,z indicate that each summation is for various hydrocarbon species with $x = 0-3$, or $y > 1$, $z \geq 0$, respectively. Thus, f_1 relates to the efficiency of defect creation by the addition of the various C_1 radical species, whereas f_2 accounts for the effect (if any) of larger hydrocarbon radical additions. Goodwin[36] showed that the defect fraction X_{def} is proportional to the growth rate G and inversely proportional to $[H]^2$, i.e., $X_{def} \sim G/[H]^2$. For his expression for G, it is seen that $X_{def} \sim [CH_3]/[H]$ for $[H] \ll 3 \times 10^{15}$ cm^{-3}. As a first approximation, we have taken $f_{1x}([CH_x]) = [CH_x]/[H]$ and considered only the effect of CH_x (*i.e.* we have assumed $f_{2yz} = 0$). For growth from CH_3 alone, eq (6) accurately describes the experimentally observed trends of $<d>$ from UNCD to SCD, as shown below. The predictions of the equations for G compared favorably with the experimental values under all UNCD, NCD, MCD and SCD growth conditions in all the hot filament CVD and MW PECVD reactors under study.

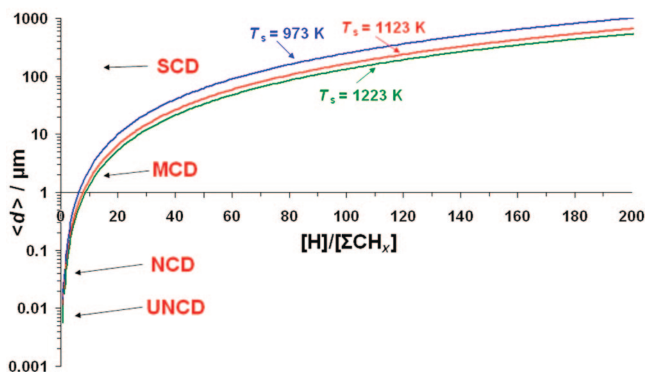

Figure 7. Log-plot of average diamond crystal size $<d>$ against the ratio of the concentrations of atomic hydrogen to all the other C_1 hydrocarbon radicals $\Sigma CH_x (x < 4)$ close to the growing diamond surface, for three substrate temperatures, T_s, calculated using eq 6 and assuming $f_2 = 0$. For the purposes of this figure, UNCD has been arbitrarily defined as diamond with crystal size <10 nm, NCD as <100 nm, and MCD < 100 nm, with SCD being an extrapolation of the lines to $<d>$ values of the order of 100s of μm or mm.

We should make it clear that the value of $<d>$ calculated here would be the *equilibrium*, *ultimate* or *limiting* value that would be achieved after the growth had occurred for sufficient length of time that any effects due to the substrate material, surface topology, and nucleation methods can be neglected. When columnar growth occurs, such as during MCD deposition, the crystal size increases with growth time. Thus, in comparing our predictions with experimental data, we must be careful to ensure that the growth time was sufficiently long that that an equilibrium between the rate of secondary nucleation and the rate of crystal size increase had been reached. For UNCD, cauliflower NCD and SCD, this is not an issue since columnar growth does not occur and crystallite size is independent of growth time.

Figure 7 shows the predictions of eq 6 as a function of $[H]/\Sigma[CH_x]$ plotted on a log-scale to allow all the diamond growth regions to be displayed on the same graph. The figure demonstrates that the type of film (SCD, MCD, NCD or UNCD) is determined simply by the $[H]/\Sigma[CH_x]$ ratio near the growing diamond surface. Low $[H]/\Sigma[CH_x]$ ratios will favor smaller crystal sizes, and thereby promote UNCD and NCD deposition. For $[H]/\Sigma[CH_x]$ values higher than 3, the crystal size approaches a few μm, so this is the MCD regime. And, extrapolating the graph, for $[H]/\Sigma[CH_x] > \sim 60$ the crystallite size becomes > 100 μm, which is approaching SCD. In this paper we shall test the predictions of eq 6 for a range of different experimental growth conditions and crystallite sizes.

3. 2D and 3D Models of Deposition Processes in HFCVD and MW PECVD Reactors. In order to study theoretically the deposition processes and compare calculated results with experimental data, we have developed 2D and 3D models of various CVD reactors which provide the values for the various parameters required in eqs 1 and 6. These parameters include the concentrations of the important hydrocarbon species near the substrate surface, and the local gas temperature. For reactors with cylindrical symmetry, a 2D model suffices, but for less symmetrical systems, such as hot filament reactors, a 3D model is needed. Normally, the two important coordinates are r, the radial distance from the center-line of the chamber, and z, the axial (vertical) height above the substrate surface. The models have been described in detail previously,[7,10,17,22] so we shall only briefly describe them here. The main model for the reactive gas mixture comprises of three blocks, which describe (i) activation of the reactive mixture (i.e., plasma parameters, power

absorption and gas heating), (ii) gas-phase processes (heat and mass transfer, species diffusion and thermal diffusion, and plasma-chemistry and plasma-chemical kinetics), and (iii) gas-surface processes (i.e., the diamond growth mechanism at the substrate surface). The energy input to the gas mixture was determined from a knowledge of the hot filament temperature[7] or from a model of the MW plasma ball.[17] The volume of the chamber was divided up into a set of smaller volume elements with grid sizes $dr = 0.5-1$ mm and $dz = 0.5-1$ mm.

The gas-phase plasma chemistry and thermochemical input for H/C/Ar mixtures are taken from various sources.[17] The plasma chemical kinetics model includes more than 200 direct and reverse reactions for 27 neutral species (C, CH, triplet-CH_2, singlet-CH_2, CH_3, CH_4, C_2(X), C_2(a), C_2H, C_2H_2, C_2H_3, C_2H_4, C_2H_5, C_2H_6, C_3, C_3H, C_3H_2, C_4, C_4H, C_4H_2, H, H_2 (v = 0,1,2), electronic excited levels H(n = 2), H(n = 3), and H_2* and six charged species (electrons, ions $C_2H_2^+$, $C_2H_3^+$, H^+, H_2^+, and H_3^+). For UNCD deposition conditions (gas mixture of 1%CH_4/(0−2%)H_2 in excess of Ar) in MW PECVD reactors, the plasma chemical kinetics was extended to include the additional ions Ar^+, ArH^+, C^+, C_2^+, C_3^+, CH^+, C_2H^+ and C_3H^+. A special procedure was developed for the calculations of the electron-molecule/atom reaction coefficients. For the range of reduced electric fields E/N and gas temperatures under study, the balance equations of plasma-chemical kinetics for charged and neutral species of H/C/Ar mixtures were solved simultaneously with the Boltzmann equation for the electron energy distribution function. As a result, the rate coefficients of the electron reactions as a function of E/N (or electron temperature T_e) and gas temperature T were obtained and used in the 2D model.

As in previous studies[7,17,37,38] the nonstationary conservation equations for mass, momentum, energy, and species concentrations, together with appropriate initial and boundary conditions, thermal and caloric equations of state, are each integrated numerically until steady-state gas temperature and radicals distributions are attained. This process yields spatial distributions of the gas temperature, T, the flow field, and the various species number densities as functions of input parameters like input power, pressure and flow rates of feed gases (e.g., H_2, Ar and CH_4). The incorporation of gas-surface reactions (see ref 18), involving H abstraction to form surface monoradical and biradical sites, and the subsequent reactions of these sites with H, H_2 and hydrocarbon radicals, plus loss and conversions of the charged species at the substrate, serve to alter the gas composition close to the surface. The main effect of these reactions is to reduce the H atom concentrations directly above the growing diamond surface, which, in turn, affects the hydrocarbon radical concentrations, growth rates and its uniformity.

3.1. Substrate−Gas Boundary Layer. The model calculates the concentrations of species above the substrate surface, but is limited in resolution to the grid size, dz, the value of which was chosen based upon the limitations of computation speed. Species concentrations *near* the substrate equates to a distance of 0.5dz in the model, but to calculate growth rates and crystal sizes using eqs 1 and 6 we require the concentrations *at* the surface. However, near the surface there is often a thin boundary layer (<1 mm) in which temperatures, gas flows and concentrations can change significantly. The chemical composition in a thin thermal boundary layer cannot be calculated accurately by a chemical mechanism with temperature-dependent reaction rates and with an assumed equilibrium thermal velocity and energy distribution based upon a given local temperature.[28] Thus, this thin boundary layer is not included in our 2D and 3D models. But for growth mechanism and growth rate calculations, the true species fluxes arriving at the substrate are required. This has been done in different ways for H atoms and for hydrocarbon species:

H Atoms. By using an approach similar to that used by Dandy et al.[39] we have taken into account[17] the substantial loss of H atoms at the substrate and substrate holder surfaces as a result of H abstraction and addition reactions. This approach provides the relationship between H atom concentrations *at* the substrate [H] and *near* the substrate $[H]_{ns}$.

Buffer Gas H_2 and Ar. For some growth conditions, e.g., for the high power density plasmas used for SCD and UNCD growth, our 2D model calculations showed that there can be a significant difference between the gas temperature near the substrate, T_{ns}, and the actual substrate temperature, T_s (e.g., T_s = 973 K, but $T_{ns} \approx 1600$ K, dz = 1 mm). As a first approach, we have assumed $[H_2] \approx [H_2]_{ns}T_{ns}/T_s$ for molecular hydrogen (and argon). The last condition of a constant mole fraction is valid for species with low reaction probabilities at the surface and in the boundary layer.

CH_3 and Other Hydrocarbons. We assume $[CH_3]$ at the surface to be approximately the same as the methyl concentration $[CH_3]_{ns}$ numerically calculated at the grid point closest to the substrate, e.g., at distance 0.5dz, where dz is the grid cell size in the axial (perpendicular to the substrate surface) direction. Similarly, we assume that for all the other hydrocarbon species $[CH_x] \approx [CH_x]_{ns}$. For hot filament CVD reactors, this approximation is justified, since there are no significant boundary layers (e.g., thermal, chemical) at the substrate surface. However, MW PECVD reactors are more complex, especially at higher powers, since a thin boundary layer could exist near to the substrate surface where there is a sharp temperature change of hundreds K over a length scale <1 mm. Nevertheless, for lack of a better model of this boundary region in MW systems we have assumed that it behaves the same as those in HF systems. In passing, we note that DC arc jet CVD reactors are even more problematic, since extremely complex nonequilibrium chemical, thermal and gas flow boundary layers exist, with temperature and axial flow velocity jumps of thousands of K and ~1 km s^{-1}, respectively.[26–28]

4. Experimental and Calculated Results for HFCVD and MW ECVD Reactors

Various CVD reactors, including our own and those whose details are available in the literature, have been simulated to try to test the predictions of the equations for G and $<d>$ over as wide a range as possible. The surface concentration approach (Section 3.1) was embedded in the developed HF and MW discharge CVD reactor models and the calculated results are given in Table 1 for each set of conditions.

(a) UNCD conditions, HFCVD reactor:[18] Films were deposited using a standard HF reactor operating at a pressure of 100 Torr using high purity Ar, CH_4, and H_2 as source gases. [Ar]/([Ar] + $[H_2]$) was kept constant at 80% and that of $[CH_4]/[H_2]$ + $[CH_4]$) at 1.5%. The filament temperature was kept constant at 2400 °C and the substrate was single crystal Si (100) which had been manually abraded prior to deposition using 100 nm diamond grit. The substrate sat on a separate heater to give additional uniform heating and to maintain it at a temperature of ~850−900 °C. Films were deposited for ~8 h to give a thickness of 0.5 μm, see Figure 8a, with grain sizes <10 nm.

(b) UNCD conditions, MW PECVD reactor: Films were deposited using a (0.5%−1%)CH_4/1%H_2/Ar gas mixture at a

TABLE 1: Concentrations (in cm^{-3}) of the Various Species *near* the Surface, and H Atoms *at* the Surface [H], Calculated for the Five Different Diamond Film Growth Conditions Given in the Text[a]

	UNCD(HF)	UNCD(MW)	NCD(HF)	MCD(HF)	SCD(MW)
T_s/K	1173	873	1173	1173	973
T_{ns}/K	1445	1335	1267	1267	1736
species					
[H] (at surface)	3.00×10^{13}	6.23×10^{14}	1.52×10^{14}	1.85×10^{14}	8.90×10^{15}
H (near surface)	1.38×10^{14}	4.85×10^{15}	2.30×10^{14}	2.86×10^{14}	3.83×10^{16}
CH_3	3.82×10^{13}	5.82×10^{10}	5.68×10^{13}	1.44×10^{13}	3.24×10^{13}
C_2H_2	2.97×10^{13}	1.66×10^{15}	2.97×10^{12}	2.44×10^{11}	2.96×10^{16}
CH_2	1.55×10^{10}	2.02×10^{9}	8.12×10^{10}	2.69×10^{10}	1.06×10^{12}
CH_2(S)	5.62×10^{8}	6.73×10^{7}	1.14×10^{9}	3.62×10^{8}	5.96×10^{10}
CH	5.28×10^{7}	2.37×10^{9}	6.53×10^{8}	2.71×10^{8}	1.60×10^{11}
C	1.05×10^{7}	1.18×10^{12}	5.45×10^{9}	3.34×10^{9}	1.41×10^{12}
C_2(a)	2.49×10^{5}	6.06×10^{11}	1.74×10^{5}	6.47×10^{4}	4.19×10^{10}
C_2(X)	1.49×10^{4}	2.19×10^{11}	5.40×10^{4}	1.38×10^{4}	1.12×10^{10}
C_2H	2.28×10^{7}	3.74×10^{12}	1.19×10^{6}	1.21×10^{5}	6.37×10^{12}
C_2H_2	2.97×10^{13}	1.66×10^{15}	2.97×10^{12}	2.44×10^{11}	2.96×10^{16}
C_2H_3	1.57×10^{10}	1.77×10^{12}	9.99×10^{9}	6.94×10^{8}	1.76×10^{13}
C_2H_4	6.93×10^{12}	2.00×10^{12}	1.94×10^{12}	1.12×10^{11}	5.82×10^{13}
C_2H_5	1.51×10^{10}	4.48×10^{8}	2.71×10^{10}	1.44×10^{9}	8.22×10^{9}
C_2H_6	6.85×10^{11}	1.11×10^{8}	9.71×10^{11}	5.12×10^{10}	2.36×10^{9}
CH_4	2.21×10^{15}	7.52×10^{10}	1.11×10^{15}	2.25×10^{14}	4.69×10^{13}
H_2	1.83×10^{17}	1.81×10^{16}	1.51×10^{17}	1.52×10^{17}	9.33×10^{17}
Ar	5.34×10^{17}	1.21×10^{18}	-	-	-
C_3	-	6.18×10^{14}	-	-	1.28×10^{14}
[H]/CH_x, $x = 0-3$	0.785	500	2.67	12.8	253.5
R	0.041	0.06	0.11	0.114	0.09
$G(CH_3)/(\mu m\ h^{-1})$	0.12	0.0006	1.4	0.42	1.97
$G(CH_x)$, $x = 0-2/(\mu m\ h^{-1})$	0.0009	0.084	0.012	0.005	0.29
<d>	8.1 nm	8 mm	94 nm	2.2 μm	1.44 mm
experimental values					
$G/(\mu m\ h^{-1})$	0.06	~0.1	~1.0	0.35	3−4
<d>	<10 nm	~15 nm	~100 nm	1−50 μm[b]	≫100 μm[c]

[b] Depends on thickness. [c] SCD over an area 2.5 mm × 2.5 mm but with some round-shaped growth structures with heights up to 0.5 μm and widths ~100 μm. [a] R is the fraction of monoradical sites, calculated using eq 4. The growth rate, G_{CH3}, is given for additions of CH_3 onto monoradical and biradical sites. Crystal sizes are calculated using eqs 6 with $f_1 = [H]/\Sigma[CH_x]$, $x = 0-3$ and $f_2 = 0$.

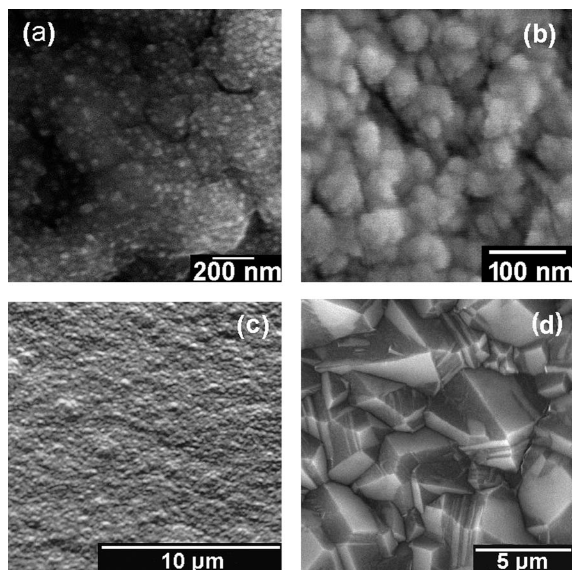

Figure 8. Scanning electron micrographs of four of the five types of diamond grown and modeled in this report. (a) UNCD(HF), (b) UNCD(MW), (c) cauliflower NCD, and (d) MCD.

pressure of 170 Torr, 700 W of input power, which heated the substrate to a temperature of 873 K. The visible extent of the plasma was estimated to be a cylinder of diameter ~4−5 cm by 5 cm high, situated directly above the substrate holder. The gas temperature was determined by fitting the rising baseline observed in optical emission spectroscopy to a blackbody radiation equation.[40] The baseline occurred since these H-poor plasmas produce small amounts of solid soot particles, especially near the cooler edges of the plasma. The soot particles achieve local thermal equilibrium with the gas, and blackbody emission from these can be used to characterize the local gas temperature at the plasma edges.[41] Gas temperatures determined in this way were ~2500 K which are not in contradiction with our calculated gas temperatures ~3200−3400 K at the center of plasma. These calculated maximum gas temperatures, together with calculated C_2 column densities ($C_2(a)_{column} \approx 1.2 \times 10^{15}$ cm^{-2}), are reassuringly consistent with the C_2 rotational temperatures ~3000−4000 K and column densities $C_{2\ column} \approx 5 \times 10^{14} - 10^{15}$ cm^{-2} measured by cavity ring down spectroscopy in similar discharge conditions.[42] These agreements give us confidence that the basic model for the gas chemistry within the reactor is accurate, and justifies the use of its predicted species concentrations in eqs 1 and 6. Our films were grown for 8 h, giving a thickness ~0.8 μm, with grain size ~15 nm, see Figure 8b.

(c) Cauliflower NCD conditions, HFCVD reactor: Films were deposited in the same reactor and under the same conditions as (a) above, except using 5%CH_4 in H_2 at 20 Torr. Films were grown for 8 h giving a film thickness of ~8 μm, with a cauliflower morphology and average grain size ~100 nm, see Figure 8c.

(d) MCD conditions, HFCVD reactor:[10] Films were deposited in the same reactor and under the same conditions as (a) above, except using 1%CH_4 in H_2 at 20 Torr. Films were grown for 8 h giving a film thickness of 2.8 μm, and exhibited a facetted morphology with crystal size ~1 μm (Figure 8d). However,

TABLE 2: Percentage of the Total Growth from Each of the Channels for the Five Types of Diamond Film Growth with Conditions Given in the Text

% contribution to G_{total}	UNCD (HF)	UNCD (MW)	NCD	MCD	SCD
G(CH_3, biradical)	70.0	0.3	59	56	13.3
G(CH_3, monoradical)	29.3	0.4	40.1	42.9	74.
G(CH_x), $x = 0-2$	0.7	99.3	0.9	1.1	12.7

due to the columnar nature of the growth, the crystal size was a function of deposition time (i.e., film thickness). The largest crystal size observed in this system was ~50 μm for a 120 μm-thick film that had been grown intermittently over a period of a few weeks - however, even this crystal size was not the true 'equilibrium' crystal size. The growth rate was too small to allow an MCD film to be grown thick enough to reach equilibrium.

(e) SCD conditions, MW PECVD reactor:[17] These films were near-SCD growth on (100) diamond substrates reported by Bogdan et al.[13] They used a 600 W MW plasma reactor at a gas pressure of 180 Torr and 10% CH_4/H_2, with a substrate temperature of 973 K. They report growth rates of 3−4 μm h^{-1} over areas of 2.5 × 2.5 mm, but with some round-shaped growth structures with heights up to 0.5 μm and widths up to 100 μm.

Table 1 summarizes the experimental and predicted values for the gas content, along with G and $\langle d \rangle$ for each of the deposition conditions and film types. [CH_3] remains relatively constant for all reactors under study, except in the case of the MW PECVD reactor for UNCD where [CH_3] is three orders lower. Comparing the 4 film types with dominant CH_3 concentrations, the first point to note is the variation in H concentration close to the surface. For NCD and MCD growth conditions, [H] $\approx 10^{14}$ cm^{-3}, whereas for UNCD in the HFCVD reactor [H] is an order of magnitude less, while for SCD conditions [H] is nearly 100 × greater. It is this variation over 3 orders of magnitude for [H] that can be considered as the prime cause of the different growth channels, and thus different film morphologies. UNCD(HFCVD) growth conditions can be regarded as 'H atom poor', whereas SCD conditions are 'extremely H atom rich'.

The concentrations of C atoms are negligible for each type of growth conditions, except for UNCD(MW PECVD) and SCD, for which [C] $\approx 10^{12}$ cm^{-3}. For UNCD(HFCVD), NCD and MCD, [CH_x, $x < 3$] ≈ 0.1% of [CH_3], but for SCD this value rises by a factor of 100 to 10%. However, the very high [H] for SCD conditions ensures that virtually all of these CH_x species which strike the surface are rapidly hydrogenated to CH_2 structures before they have a chance to cross-link. The way to see this is by looking at the values for [H]/Σ[CH_x], $x < 4$, which rise rapidly from less than 1 to nearly 200 on going from UNCD(HFCVD) to SCD growth conditions. The UNCD(MW PECVD) case is discussed below.

The values for the open site density for monoradical sites, R, and biradical sites, R^2, remain at around 4%−11% and ~0.16%−1%, respectively, for all growth regimes. The lowest values of $R \approx$ 4%−6% are realized for UNCD(HFCVD and MW) and help to explain the low growth rates observed for UNCD.

Comparing the calculated and experimental growth rates, we find that G_{total} predicts the experimental growth rates very accurately for *all* the types of growth, to within a factor of ~2. Table 2 shows the contribution to the total growth rate from each of the three channels considered within the growth model. For all film types except UNCD(MW PECVD), CH_3 is the major growth species, with CH_x ($x < 3$) species contributing only ~1%−13% of the carbon in the diamond lattice. For UNCD(HF-CVD), NCD and MCD, growth occurs via CH_3 addition to both biradical and monoradical sites, but the relative amounts of each vary greatly. For UNCD(HF), the majority of the growth (70%) is from addition of CH_3 to biradical sites, whereas the converse happens for SCD, where ~74% of the growth is from CH_3 adding to monoradical sites.

Comparing the calculated equilibrium crystal sizes in Table 1, we see that growth rate eqs 1, 3, and 5 predict values that are consistent with the experimental values for all the forms of diamond. Equation 6 predicts well the values of the experimental crystal sizes for all the forms of diamond, except UNCD in the MW PECVD reactor. It predicts that the equilibrium crystal size for MCD conditions is ~2.2 μm, which is smaller than the value expected from extrapolating the experimental values from a few 10s of hours to much longer deposition times, although still a reasonable estimate given that the exact definition and meaning of $\langle d \rangle$ for facetted, columnar growth is somewhat vague. Equation 6 also predicts that $\langle d \rangle$ for the SCD conditions is ~0.14 mm, which is consistent with the experimental reports given that large defects were created on the (near) SCD surface.

UNCD growth in the MW PECVD reactor is the only case where eq 6 does not predict the crystal size accurately, and is also the only case with the dominant growth species being something other than CH_3. As our calculations show, the atomic C concentration of [C] $\approx 10^{12}$ cm^{-3} is sufficient to account for the observed experimental low growth rates. Despite the low total hydrogen percentage in the feed gas (~2%H_2 for our base mixture 0.5%CH_4/1%H_2/Ar), these growth conditions are not actually hydrogen poor, since the calculated atomic hydrogen concentration at the substrate [H] $\approx 6 \times 10^{14}$ cm^{-3}. This is because high gas temperatures ~3300−3400 K in the center of plasma region lead to complete dissociation of CH_4 and substantial H_2 dissociation (mole fractions $X_{H2} \approx 0.16\%$). As a result, we get high mole fractions of C atoms, C_2, C_3 molecules and H atoms in the hot plasma core (~0.09%, 0.06%, 0.08% and 2.7%, respectively) and above the substrate. The remaining disagreement between experimental measurements and our theoretical predictions of $\langle d \rangle$ may be due to secondary growth processes that are not included in the model. These could be factors such as (i) unknown specific features of the C atom growth mechanism, (ii) a high nucleation density, and/or (iii) a possible increased rate of renucleation due to other hydrocarbon species (e.g. C_2, C_2H, C_3, C_3H), so that $f_2 \neq 0$ in eq 6. In fact, by using the empirically derived factor $f_2 = 2000([C_2]/[CH_x])^2$, we find that eq 6 predicts all five cases of diamond growth considered here, including the problematic UNCD(MW PECVD). However, as yet we have no rationalization for the defect-creation mechanisms that might give rise to a function of this form, and this requires further study.

5. Conclusions

In this paper we have presented further evidence to support and refine our model[9,10,17,18] for the growth mechanisms of the various forms of diamond film. Knowledge of the gas phase concentrations near the growing diamond surface can be used to estimate the growth rate and average crystal size during diamond CVD, and thereby to predict whether the film morphology will be UNCD, NCD, MCD or SCD. In summary, we can deduce that growth of diamond is a sliding scale, with different types of diamond arising from a smoothly changing ratio of atomic H to hydrocarbon radicals at the growing surface. The different growth conditions, gas mixtures, temperatures and

pressures reported in the literature for diamond growth, simply serve to fix the value of this ratio [H]:$\sum CH_x$], and with it, the resulting film morphology and growth rate. As a general rule, we can say that:

UNCD conditions in a HFCVD reactor: growth is dominated by CH_3 addition to biradical sites, with a small contribution from CH_3 addition to monoradical sites. The low concentrations of CH_3 as well as mono and biradical sites account for the low growth rate of UNCD. The relatively low concentration of H near the surface slows down the rate of three-body recombination ($H + CH_3 + M$) and thus allows CH_3 to survive at low substrate temperatures, as mentioned above, and also allow reactive adducts to survive longer on the surface. Thus, cross-linking reactions occur readily, leading to a high number of renucleation events and small (nm-sized) crystal sizes.

UNCD conditions in a MW PECVD reactor: growth is dominated by C addition to monoradical sites, with a small contribution from CH_3 addition. The low concentrations of C atoms ($\sim 10^{12}$ cm^{-3}) and CH_3 ($\sim 6 \times 10^{10}$ cm^{-3}) radicals can account for the experimentally observed low growth rate of UNCD, although our model (which is based upon CH_3 being the main growth species) fails to predict the small crystallite size. This needs further theoretical and experimental study in order to understand the mechanisms for renucleation under these unusual conditions.

NCD conditions: growth is still dominated by CH_3 addition to biradical sites, although there is now a much larger contribution from monoradical sites. Thus, the growth rate is much higher than for UNCD, and the higher H concentration means that more of the reactive adducts are hydrogenated to CH_2 before they can cross-link. The atomic H at the surface catalyzes the migration of CH_2 groups across the (100) surface until they meet a step-edge and lock into the lattice. This competes with the renucleation processes, and the effect is that the average crystallite size increases to 10s or 100s of nm.

MCD conditions: growth is now (almost) equally shared between CH_3 addition to biradical and monoradical sites. [H] is higher still, so nearly all of the reactive adducts are hydrogenated to CH_2 before they can cross-link, producing much larger terraces, with only occasional renucleation, and ultimately leading to facetted, micron-sized crystallites.

SCD conditions: the concentration of atomic H at the surface is now so high that growth is dominated by CH_3 addition to monoradical sites. Since these sites are in abundance, this leads to a greatly increased growth rate. The high [H] also ensures the fast surface migration of CH_2 groups[20] and rapid hydrogenation of CH_x adducts to CH_2 bridging groups. Thus, growth is solely from CH_2 migration to step-edges, leading to large crystallites of size several mm.

We can predict from these findings that to grow still larger SCD, say into the cm scale, a reactor would need to be designed that could produce ratios of [H]/[CH_3] of $>200-300$, while maintaining a surface temperature of ~ 700 °C. Alternatively, by decreasing this ratio to <1, it might be possible to synthesize the larger diamondoid molecules,[43] albeit encased in the form of a thin film. UNCD deposition conditions in argon rich mixtures in MW PECVD reactors require further theoretical and experimental study.

Although the results presented here seem to indicate that growth of all types of diamond can now broadly be explained, a word of caution is advised. We have not considered the effects of nitrogen upon either the gas chemistry or upon the surface reactions. Nitrogen, even as an unwanted impurity at the ppm level, is known to significantly effect growth rates and film morphology. Nor have we considered oxygen-, halogen-, or boron-containing gas mixtures, which also affect many aspects of growth. Nevertheless, we feel that the results in this paper give a valuable insight into the physical and chemical processes underlying diamond growth, and hopefully will provide some pointers to advance this technology further, in terms of higher growth rates, with higher purity, and larger crystals.

Acknowledgment. The authors thank James Butler plus the members of the Bristol diamond group for useful discussions, and Oliver Fox for the SEM of MW-grown UNCD. Y.A.M. thanks the RF government for Key Science Schools Grant No. 133.2008.2 and ISTC for Grant No. 2968/2005.

References and Notes

(1) May, P. W. *Phil. Trans. R. Soc. Lond. A* **2000**, *358*, 473.
(2) Harris, S. J. *Appl. Phys. Lett.* **1990**, *56*, 2298.
(3) Goodwin, D. G. and Butler, J. E., *in:*, M. A., Prelas, G., Popovici, L. K., Bigelow Eds.), Handbook of Industrial Diamonds and Diamond Films (, Marcel Dekker, New York, 1998).
(4) Gruen, D. M., Shenderova, O. A., Ya. Vul′, A. Eds.), , *Synthesis, Properties and Applications of Ultrananocrystalline Diamond*, Springer, 2005, NATO Science Series part II, vol. 192).
(5) Xiao, X.; Birrell, J.; Gerbi, J. E.; Auciello, O.; Carlisle, J. A. *J. Appl. Phys.* **2004**, *96*, 2232.
(6) Williams, O. A.; Daenen, M.; D'Haen, J.; Haenen, K.; Maes, J.; Moshchalkov, V. V.; Nesládek, M.; Gruen, D. M. *Diamond Relat. Mater.* **2006**, *15*, 654.
(7) May, P. W.; Smith, J. A.; Mankelevich, Yu. A. *Diamond Relat. Mater.* **2006**, *15*, 345.
(8) Zhou, D.; McCauley, T. G.; Qin, L. C.; Krauss, A. R.; Gruen, D. M. *J. Appl. Phys.* **1998**, *83*, 540.
(9) May, P. W.; Harvey, J. N.; Smith, J. A.; Mankelevich, Y. A. *J. Appl. Phys.* **2006**, *99*, 104907.
(10) May, P. W.; Mankelevich, Yu. A. *J. Appl. Phys.* **2006**, *100*, 024301.
(11) Rabeau, J. R.; John, P.; Wilson, J. I. B.; Fan, Y. *J. Appl. Phys.* **2004**, *96*, 6724.
(12) Bogdan, G.; Nesládek, M.; D'Haen, J.; Maes, J.; Moshchalkov, V. V.; Haenen, K.; D'Olieslaeger, M. *Phys. Stat. Solidi A* **2005**, *202*, 2066.
(13) Bogdan, G.; De Corte, K.; Deferme, W.; Haenen, K.; Nesládek, M. *Phys. Stat. Solidi A* **2006**, *203*, 3063.
(14) Isberg, J.; Hammersberg, J.; Johansson, E.; Wikström, T.; Twitchen, D. J.; Whitehead, A. J.; Coe, S. E.; Scarsbrook, G. A. *Science* **2002**, *297*, 1670.
(15) Yan, C.-s.; Mao, H.-k.; Li, W.; Qian, J.; Zhao, Y.; Hemley, R. J. *Phys. Stat. Solidi A* **2004**, *201*, R25.
(16) Ho, S. S.; Yan, C. S.; Liu, Z.; Mao, H. K.; Hemley, R. J. *Ind. Diamond Rev. Jan* **2006**, 28.
(17) Yu., A. Mankelevich, P. W. May, , Diamond Relat. Mater. 2008, in press).
(18) May, P. W.; Ashfold, M. N. R.; Mankelevich, Yu. A. *J. Appl. Phys.* **2007**, *101*, 053115.
(19) Silva, F.; Bonnin, X.; Achard, J.; Brinza, O.; Michau, A.; Gicquel, A. *J. Cryst. Growth* **2008**, *310*, 187.
(20) Skokov, S.; Weiner, B.; Frenklach, M. *J. Phys. Chem.* **1994**, *98*, 7073.
(21) Mankelevich, Y. A.; Suetin, N. V.; Ashfold, M. N. R.; Boxford, W. E.; Orr-Ewing, A. J.; Smith, J. A.; Wills, J. B. *Diamond Relat. Mater.* **2003**, *12*, 383.
(22) Mankelevich, Y. A.; Rakhimov, A. T.; Suetin, N. V. *Diamond Relat. Mater.* **1996**, *5*, 888.
(23) Harris, S. J.; Goodwin, D. G. *J. Phys. Chem.* **1993**, *97*, 23.
(24) Zhang, Y. F.; Dunn-Rankin, D.; Taborek, P. *J. Appl. Phys.* **1993**, *74*, 6941.
(25) Yamada, H.; Chayahara, A. Yoshiaki Mokuno, Y. Horino, N. Fujimori. *Diamond Relat. Mater.* **2006**, *15*, 522.
(26) Coltrin, M. E.; Dandy, D. S. *J. Appl. Phys.* **1993**, *74*, 5803.
(27) Yu, B. W.; Girshick, S. L.; Appl, J. *Phys.* **1994**, *75*, 3914.
(28) Yu., A.; Mankelevich, A. J.; Orr-Ewing, M. N. R.; Ashfold, *J. Appl. Phys.* **2007**, *102*, 063310.
(29) Fujii, T.; Kareev, M. *J. Appl. Phys.* **2001**, *89*, 2543.
(30) Eckert, M.; Neyts, E.; Bogaerts, A. *J. Phys. D: Appl. Phys.* **2008**, *41*, 032006.
(31) Kondoh, E.; Ohta, T.; Mitomoto, T.; Ohtsuka, K. *Appl. Phys. Lett.* **1991**, *59*, 488.
(32) Petherbridge, J. R.; May, P. W.; Pearce, S. R. J.; Rosser, K. N.; Ashfold, M. N. R. *J. Appl. Phys.* **2001**, *89*, 1484.
(33) Pradhan, D.; Lee, Y. C.; Pao, C. W.; Pong, W. F.; Lin, I. N. *Diamond Relat. Mater.* **2006**, *15*, 2001.

(34) Smith, G. P. Golden, D. M. Frenklach, M. Moriarty, N. W. Eiteneer, B. Goldenberg, M. Bowman, C. T. Hanson, R. K. Song, S. Gardiner, Jr., W. C. Lissianski, V. V. Qin, Z. http://www.me.berkeley.edu/gri−mech/.

(35) Frenklach, M.; Skokov, S. *J. Phys. Chem B* **1997**, *101*, 3025.

(36) Goodwin, D. G. *J. Appl. Phys.* **1993**, *74*, 6888.

(37) Ashfold, M. N. R.; May, P. W.; Petherbridge, J. R.; Rosser, K. N.; Smith, J. A.; Mankelevich, Y. A.; Suetin, N. V. *Phys. Chem. Chem. Phys.* **2001**, *3*, 3471.

(38) Smith, A. ; Wills, J. B. ; Moores, H. S. ; Orr-Ewing, A. J. ; Yu., A. ; Mankelevich, N. ; Suetin, V. *J. Appl. Phys.* **2002**, *92*, 672.

(39) Dandy, D. S. ; Coltrin, M. E. *J. Mater. Res.* **1995**, *10*, 1993.

(40) Elliott, M. A.; May, P. W.; Petherbridge, J.; Leeds, S. M.; Ashfold, M. N. R.; Wang, W. N. *Diamond Relat. Maters.* **2000**, *9*, 311.

(41) Hassouni, K.; Mohasseb, F.; Bénédic, F.; Lombardi, G.; Gicquel, A. *Pure Appl. Chem.* **2006**, *78*, 1127.

(42) Lombardi, G.; Bénédic, F.; Mohasseb, F.; Hassouni, K.; Gicquel, A. *Plasma Sources Sci. Technol.* **2004**, *13*, 375.

(43) Filik, J.; Harvey, J. N.; Allan, N. L.; May, P. W.; Dahl, J. E. P.; Liu, S.; Carlson, R. M. K. *Phys. Rev. B* **2006**, *74*, 035423.

JP803735A